JJMIE

Volume 4, Number 1, Jan.2010
ISSN 1995-6665
Pages 193 - 204

Jordan Journal of Mechanical and Industrial Engineering

Transient Analysis and Output Characteristics of DC Motors Fed by Photovoltaic Systems

Mohammad S. Widyan [a,*], Anas I. Al Tarabsheh [a], Issa Y. Etier [a], Rolf E. Hanitsch [b]

[a] *Electrical Engineering Department , The Hashemite University, 13115 Zarqa, Jordan*

[b] *Institute of Energy and Automation Technology , Berlin University of Technology,Einsteinufer 11, D-10587 Berlin , Germany*

.

Abstract

This paper presents the dynamical analysis of DC shunt, series and permanent-magnet PM motors fed by photovoltaic PV energy systems at different illuminations. At the full solar intensity, the maximum power point of current/voltage I/V characteristic of the PV modules is designed to be at the rated conditions of the machines. The nonlinear behavior of I/V characteristics of the PV modules and that of the magnetization curve of the ferromagnetic materials of the machines are approximated by polynomial curve fitting. The dynamical analysis of the machines fed by fixed terminal voltage has also been carried out and a comparison between the cases of supplying the motors by fully illuminated solar cells, partially illuminated solar cells and fixed terminal voltage is addressed. The steady-state output characteristics, the torque-speed characteristics, of the three DC motors with the two inputs are presented and compared.

Keywords: Dynamical Analysis of DC machines; Photovoltaic Cells; Steady-State Output Characteristics.

1. Introduction

DC motors are electrical machines that consume DC electrical power and produce mechanical torque. Historically, DC machines are classified according to the connection of the field circuit with respect to the armature circuit. In shunt machines, the field circuit is connected in parallel with the armature circuit while DC series machines have the field circuit in series with the armature where both field and armature currents are identical. Permanent-magnet machines, on the other hand, have only one circuit (armature winding) and the flux generated by the magnets is constant. Compared with conventional electrical machines, permanent-magnet machines exhibit higher efficiency, higher power to weight ratio and simpler construction.

The use of PV systems as a power source for electrical machines is considered a promising area in photovoltaic applications due to the ongoing growth of PV-market [1]. The dynamical and steady-state characteristics of PV-powered DC motors at different solar intensities, different loading conditions and different system controllers & configurations have been proposed [2]-[8]. Similar studies for permanent-magnet and AC machines are presented [9]-[13]. PV arrays comprise several parallel/series connected solar cells to provide sufficiently high output power for operating common loads and devices [14]. In this paper, the main contributions are the dynamical analysis and the steady-state output characteristics of DC shunt, series and permanent-magnet motors fed by photovoltaic cells at different solar intensities as compared with the case of supplying the motors by fixed terminal voltage. Additionally, the maximum power point of the photovoltaic cells is designed to be at the rated conditions of the machines when the PV array is fully illuminated. The nonlinearity of the magnetization curve of the ferromagnetic materials of the machines in case of shunt and series motors and that of the *I/V* characteristics of the photovoltaic cells have been included by polynomial curve fitting. The steady-state output characteristics when the motors are fed by solar cells at different illuminations and fixed terminal voltage have been depicted and compared for the three motors. The paper is structured as follows: The nonlinear dynamical model of the DC shunt, series and permanent-magnet motors are presented in Section II. Section III outlines the design and main characteristics of the photovoltaic cells. The numerical simulation results are addressed in Section IV. Section V depicts the steady-state output characteristics of the three machines fed by fixed voltage and by photovoltaic cells at two solar intensities. Finally, conclusions are drawn in Section VI.

Corresponding Author. mohammadwidyan@yahoo.com

2. Dynamical Model of DC Shunt, Series and Permanent-Magnet Motors

This section presents the dynamical model of the DC shunt, series and permanent-magnet motors including the nonlinearity of the magnetization curve of the ferromagnetic materials.

a) DC Shunt Motor

In shunt machine, the field circuit is connected in parallel with the armature circuit. It has the following equivalent circuit:

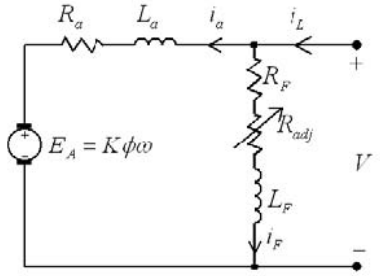

Figure 1. Equivalent Circuit of DC Shunt Motor

The equation of the field circuit is:

$$L_F \frac{di_F}{dt} = V - (R_F + R_{adj})i_F \quad (1)$$

where L_F: field winding inductance, i_F: field current, V: terminal voltage and $R_F + R_{adj}$: field winding resistance. The equation of the armature circuit is:

$$L_a \frac{di_a}{dt} = V - R_a i_a - K\phi\omega \quad (2)$$

where L_a: armature winding inductance, i_a: armature current, R_a: armature resistance, K: constant related to the design of the machine, ϕ: flux per pole and ω: rotational speed of the rotor. The motion equation of the motor is:

$$J \frac{d\omega}{dt} = K\phi i_a - T_L \quad (3)$$

where J: rotor and load moment of inertia and T_L: load torque.

The magnetization curve is the relation between the flux ϕ and the field current i_F. However, it is usually obtained experimentally in terms of the induced voltage $E_A = K\phi\omega$ as function of i_F at a certain rotational speed ω at no load. In this paper, $K\phi$ is expressed as function of the field current i_F based on the data given in [15] after dividing the induced voltage $E_A = K\phi\omega$ by the given rotational speed. $K\phi$ as function of i_F has then been polynomially fitted using MATLAB. It is found that the following second order polynomial is accurate enough to represent them as:

$$K\phi = \alpha_1 i_F^2 + \alpha_2 i_F + \alpha_3 \quad (4)$$

where $\alpha_1 = -0.3084$, $\alpha_2 = 1.0272$ and $\alpha_3 = 0.0049$.

Substituting for $K\phi$ in Eq. (2) yields:

$$L_a \frac{di_a}{dt} = V - R_a i_a - (\alpha_1 i_F^2 + \alpha_2 i_F + \alpha_3)\omega \quad (5)$$

and for $K\phi$ in Eq. (3) gives:

$$J \frac{d\omega}{dt} = (\alpha_1 i_F^2 + \alpha_2 i_F + \alpha_3) i_a - T_L \quad (6)$$

Eqs. (1), (5) and (6) represent the nonlinear dynamical behavior of a DC shunt motor including the nonlinearity of the magnetization curve of the ferromagnetic material of the machine.

b) DC Series Motor

DC series motor, with its own characteristics of high starting torque which makes it suitable for high inertia as well as traction systems, has a nonlinear dynamical model. As its name indicates, the field circuit is connected in series with the armature and therefore the armature and field currents are the same. The equivalent circuit of a DC series motor is:

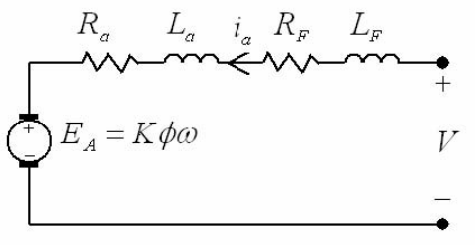

Figure 2. Equivalent Circuit of DC Series Motor

The equation of the armature:

$$(L_F + L_a)\frac{di_a}{dt} = V - (R_a + R_F)i_a - K\phi\omega \quad (7)$$

where L_F: field winding inductance, L_a: armature winding inductance, i_a: armature current, V: applied terminal voltage, R_a: armature winding resistance, R_F: field winding resistance, K: constant depends of the design of the machine, ϕ: flux per pole and ω: rotational speed of the rotor. The motion equation is:

$$J \frac{d\omega}{dt} = K\phi i_a - T_L \quad (8)$$

where J: rotor and load moment of inertia and T_L: load torque.

Based on the data presented in [15] and using MATLAB, it is found that $K\phi$ can be expressed as function of i_a as:

$$K\phi = \beta_1 i_a^2 + \beta_2 i_a + \beta_3 \quad (9)$$

where $\beta_1 = -0.0017$, $\beta_2 = 0.0938$ and $\beta_3 = 0.0062$.

Substituting for $K\phi$ in Eq. (7) yields:

$$(L_F+L_a)\frac{di_a}{dt}=V-(R_a+R_F)i_a-(\beta_1 i_a^2+\beta_2 i_a+\beta_3)\omega \quad (10)$$

and for $K\phi$ in Eq. (8) yields:

$$J\frac{d\omega}{dt}=(\beta_1 i_a^2+\beta_2 i_a+\beta_3)i_a-T_L \quad (11)$$

Eqs. (10) and (11) represent the nonlinear dynamical behavior of a DC series motor including the nonlinearity of the ferromagnetic material of the machine.

c) Permanent-Magnet DC Motor

Due to absence of the field current and field winding, permanent magnet machines exhibit high efficiency in operation, simple and robust structure in construction and high power to weight ratio. The attractiveness of the permanent-magnet machines is further enhanced by the availability of high-energy rare-earth permanent-magnet materials like SmCo and NdFeB [16]. However, the speed control of permanent-magnet DC motor via changing the field current is not possible. The equivalent circuit of the permanent-magnet DC motor is:

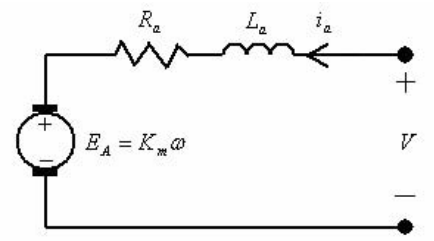

Figure 3. Equivalent Circuit of Permanent-Magnet DC Motor

Applying KVL provides the armature equation as:

$$L_a\frac{di_a}{dt}=V-R_a i_a-K_m\omega \quad (12)$$

where L_a: armature winding inductance, i_a: armature current, V: terminal voltage, R_a: armature resistance, K_m: constant related to the design of the machine and ω: rotational speed. The motion equation is:

$$J\frac{d\omega}{dt}=K_m i_a-T_L \quad (13)$$

where J: rotor and load moment of inertia and T_L: load torque. Eqs. (12) and (13) represent the dynamical model of permanent-magnet DC motor.

The complete numerical parameters of the DC shunt, series and permanent-magnet motors are given in appendix A.

3. Photovoltaic Cells Design and Main Characteristics

Figure 4, (a) shows an example of a commercial amorphous silicon (a-Si:H) PV module where twelve single p-i-n cells are incorporated. Figure 4,(b) presents the equivalent circuit generally applied for photovoltaic modules; it consists of 12 current sources in parallel to 12 diodes. Including the resistive elements and in the circuit of Figure 4, (b) represents very well the behavior of real solar cells [17] and [18]. As a simplification, the PV module is represented as a symbol shown in Figure 4, (c). The specifications of this module are listed in Table I. To increase the voltage and current capabilities of the PV cells, modules are connected in parallel and series as shown in Figure 5.

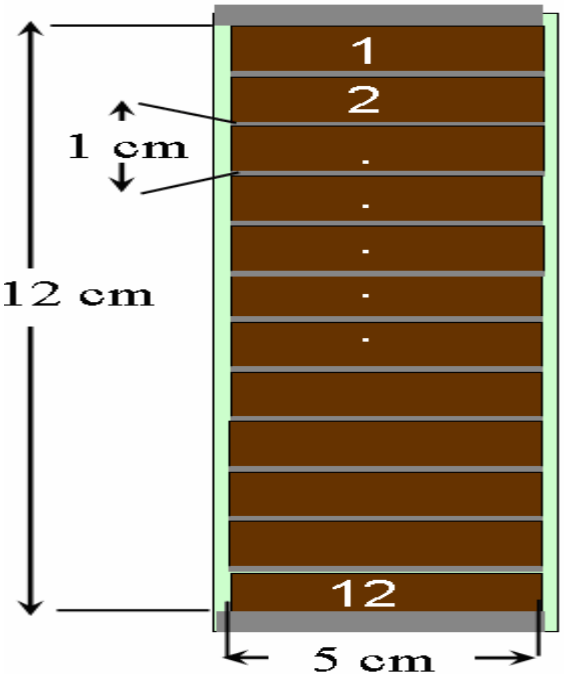

(a)

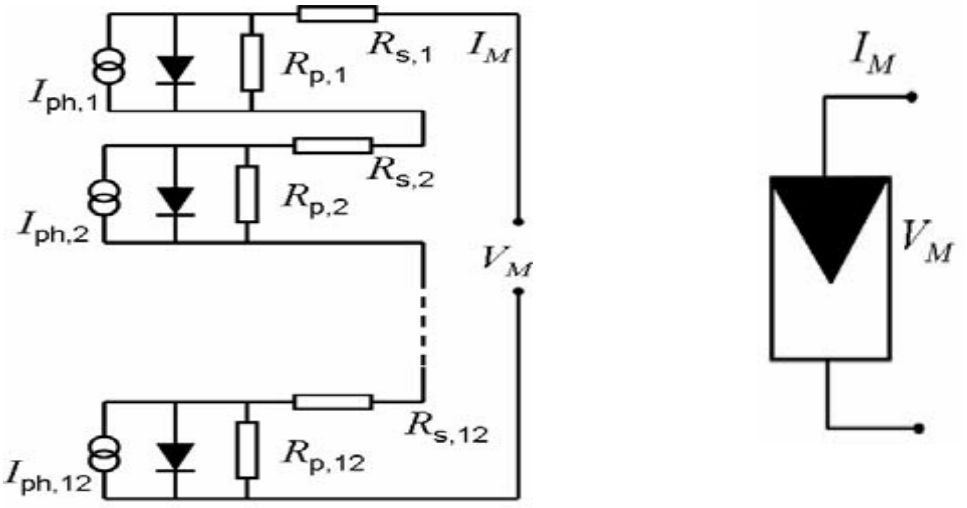

(b) (c)

Figure 4. (a) Thin film amorphous silicon a-Si:H PV module consisting of 12 series-connected solar cells (b) its equivalent circuit and (c) its symbol. The effective area of the module is $60cm^2$ where the area of each cell is $5cm^2$.

Table I. Specifications of the PV module shown in Figure 4

Nominal power (mW)	Voltage at max. power (V)	Current at max. power (mA)	Short circuit current (mA)	Open circuit voltage (V)	Dimensions (cm^2)
431	6.78	63.55	74.2	9.15	5×12

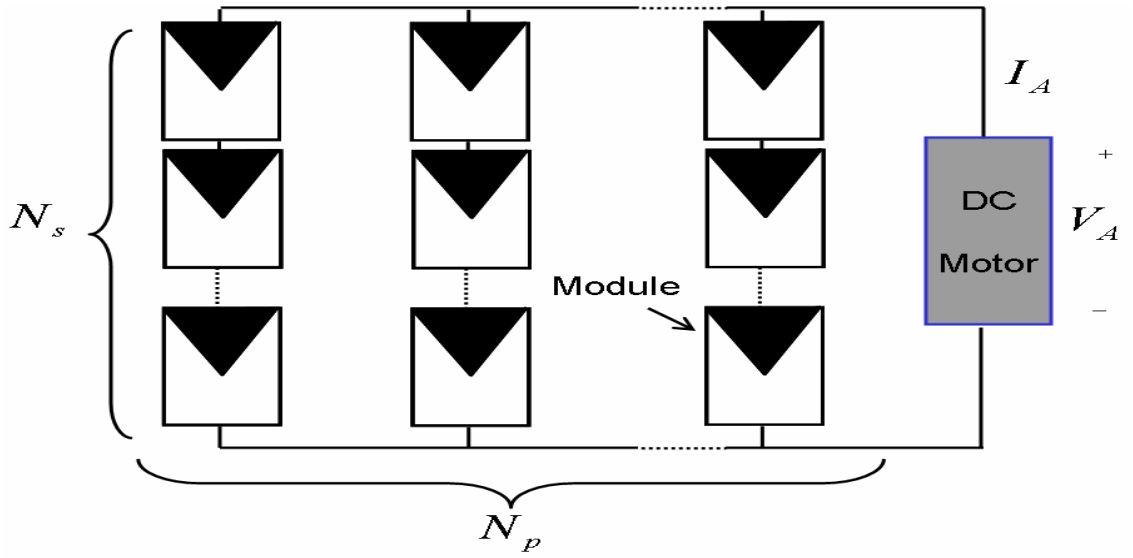

Figure 5. A PV array consisting of series- and parallel-connected modules loaded by dc motor

The I/V characteristics of the PV module are expressed as:

$$I_M = I_0 \exp\left\{\frac{V_M - I_M R_s}{n_M V_t} - 1\right\} + \frac{V_M - I_M R_s}{R_p} - I_{phM} \quad (14)$$

where I_M is the output current of the module, I_0 is the reverse-saturation current, V_M is the output voltage of the module, R_s is the series resistance per module, n is the ideality factor per module, V_t is the thermal voltage equals 25.9 mV at T=300K, R_p is the parallel resistance per module and I_{phM} is the generated current per module. Therefore, the relationship between the current and the voltage of a PV array is written as:

$$I = N_p \left(I_0 \exp\left\{ \frac{\frac{V}{N_s} - \frac{I}{N_p} R_s}{n_A V_t} - 1 \right\} + \frac{\frac{V}{N_s} - \frac{I}{N_p} R_s}{R_p} - I_{phM} \right) \quad (15)$$

In this paper, the rated conditions of the load are 130V and 16A. To generate this rated values and are selected as shown in Table II.

Table II. Parameters of the designed PV array

Design voltage (V)	Design current (A)	N_s	N_p	Area of PV array (m^2)
130	16	19	252	5.8

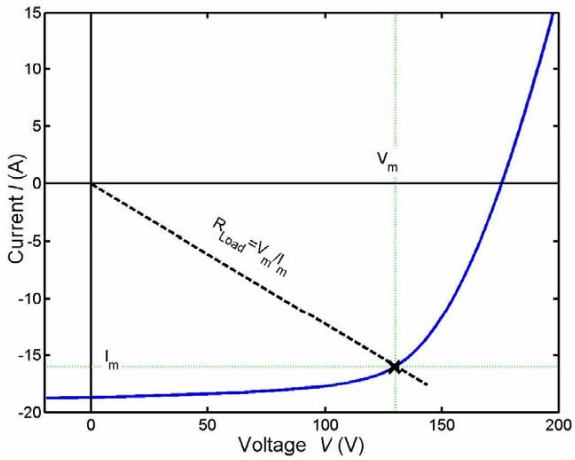

Figure 6. Current/voltage characteristics of the designed PV array consisting of 19 series- and parallel-connected modules

Apparently, the output characteristic of the photovoltaic cells is highly nonlinear. Using the MATLAB instruction 'polyfit' it is found that a polynomial of the 9^{th} order is accurate enough to represent the output voltage as function of the current at full illumination as:

$$V = \gamma_1 I^9 + \gamma_2 I^8 + \gamma_3 I^7 + \gamma_4 I^6 + \gamma_5 I^5 + \gamma_6 I^4 + \gamma_7 I^3 + \gamma_8 I^2 + \gamma_9 I + \gamma_{10} \quad (16)$$

where V is the terminal voltage of the photovoltaic cells, I is the output current, $\gamma_1 = -1.352 \times 10^{-6}$, $\gamma_2 = 1.0779 \times 10^{-4}$, $\gamma_3 = -3.5926 \times 10^{-3}$, $\gamma_4 = 6.4851 \times 10^{-2}$, $\gamma_5 = -0.6865$, $\gamma_6 = 4.3097$, $\gamma_7 = -15.4538$, $\gamma_8 = 28.6745$, $\gamma_9 = -24.1155$ and $\gamma_{10} = 179.9758$.

Fig. 7 shows the polynomially fitted V/I characteristics of the designed cells at different illuminations. The terminal voltage V of Eqs. (1), (5), (10) and (12) is replaced by the expression of Eq. (16) when the motors are fed by photovoltaic cells. In shunt motor, I represents $i_F + i_a$ and in series & permanent-magnet motors I represents i_a.

IV. Numerical Simulations

The numerical simulation results of the DC shunt, series and permanent-magnet motors are presented in this section.

a) DC Shunt Motor

Figure 8, (a) shows the field current of the DC shunt motor after a step change in the load torque from 5Nm to the rated torque of 10.4Nm subjected at $t = 5s$ for the two cases of fixed terminal voltage and a terminal voltage supplied by the photovoltaic cells at full solar illumination and 0.75 of the full illumination with a field resistance of $100\,\Omega$. As the load increases, the current withdrawn by the motor increases. The terminal voltage of the photovoltaic cells decreases as a result. At light loads, the terminal voltage of the photovoltaic cells is higher than the nominal voltage of the machine. This justifies the higher field current at the light load of 5Nm in case of photovoltaic cells. The armature current is shown in Figure 8, (b) and the corresponding rotational speed is shown in Figure 8, (c). In all responses, the steady-state values at the rated load torque are in good agreement at full illumination as the photovoltaic cells are designed to provide the rated voltage at the rated current of the motor at the full solar illumination. At 0.75 of the full illumination the response is lower than that when the motor is fed by fixed terminal voltage and so is the rotational speed as shown in Figure 9, (b).

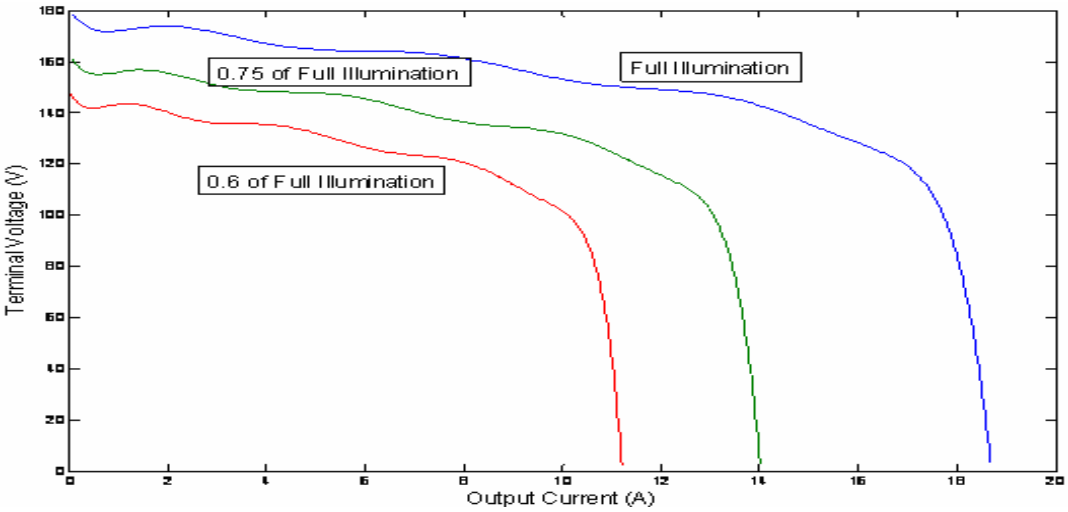

Fig 7: Polynomially fitted I/V characteristics of the designed photovoltaic array at different illuminations

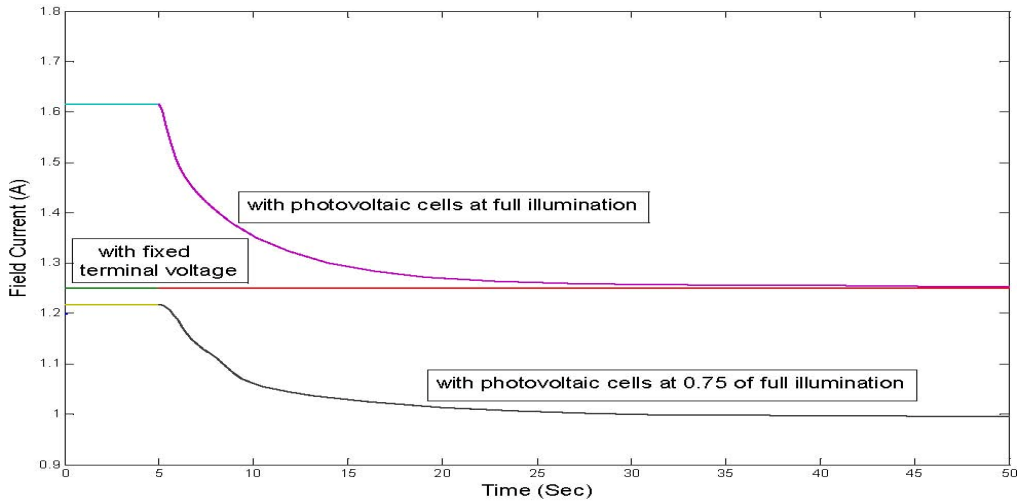

(a)

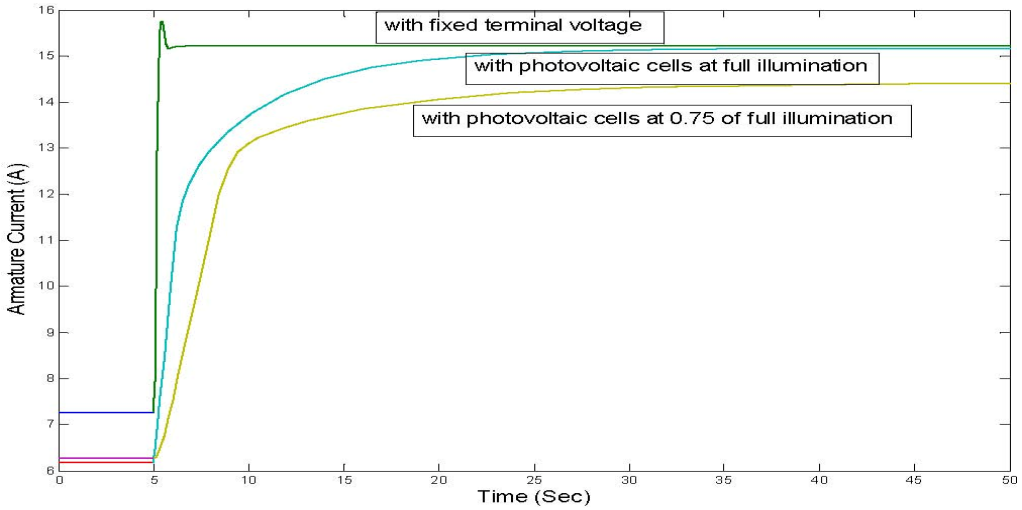

(b)

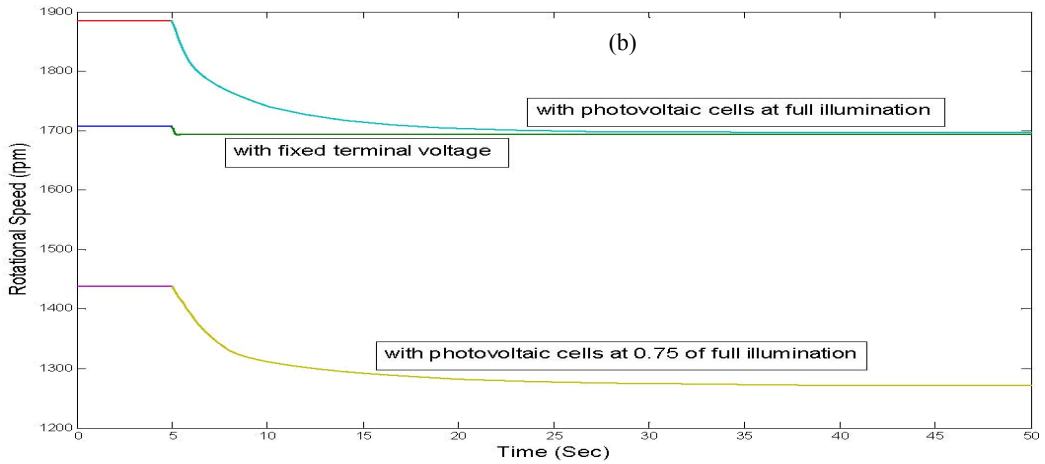

(c)

Figure 8. (a) Field current, (b) armature current and (c) rotational speed of DC shunt motor after a step change on the load torque from 5Nm to 10.4Nm with a total field resistance of 100 Ω

b) DC Series Motor

The simulations executed on the DC shunt motor are repeated for the series motor. Figure 9, (a) shows the armature current of the series motor after a step increase in the load torque from 5Nm to 17Nm for the cases of fixed terminal voltage and a terminal voltage supplied by photovoltaic cells at full solar illumination and 0.75 of the full illumination. The steady-state armature current in case of photovoltaic cells and full illumination is slightly higher These small deviations are justified by the small difference in the voltage supplied by the photovoltaic cells compared with the fixed rated voltage of 125V as shown in Figure 9, (c). This difference comes as result of the fact that the output voltage of the photovoltaic cells is function of the output current. At 0.75 of the full illumination the response is lower.

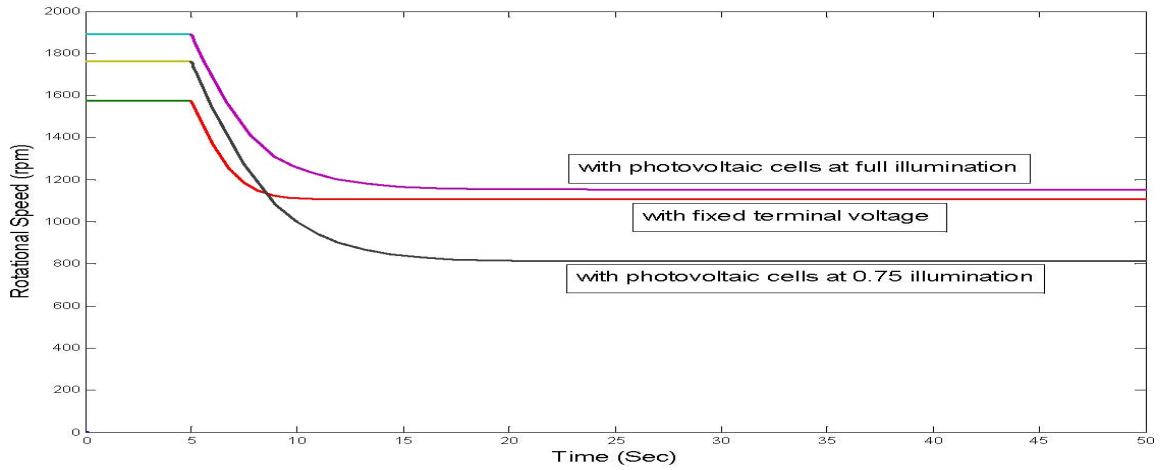

(a)

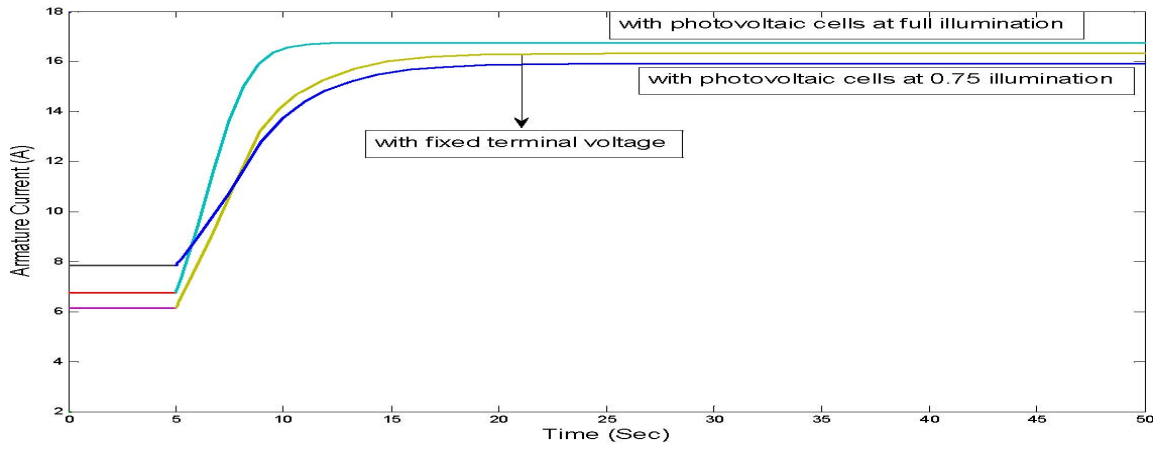

(b)

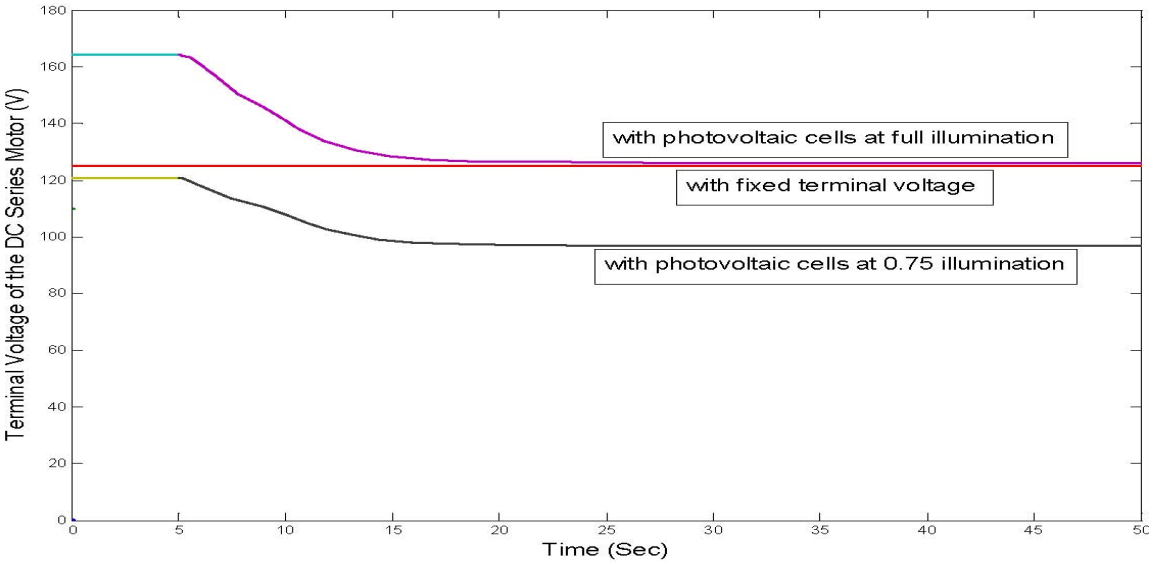

(c)

Figure 9: (a) Armature current, (b) rotational speed and (c) terminal voltage (photovoltaic cells voltage) of the DC series motor after a step increase in the load torque from 5Nm to 17Nm

c) Permanent-Magnet DC Motor

Figure 10, (a) shows the armature current of the permanent-magnet DC motor after a step increase in the load torque from 5Nm to 11.9Nm for the cases of fixed terminal voltage and a terminal voltage supplied by photovoltaic cells at full solar illumination and 0.75 of the full illumination. The steady-state armature current in case of photovoltaic cells and fixed terminal voltage is identical because it is independent of the input voltage as can be concluded from Eq. (13). The deviation in the rotational speed shown in Figure 10, (b) comes as a result of the difference in the applied voltage.

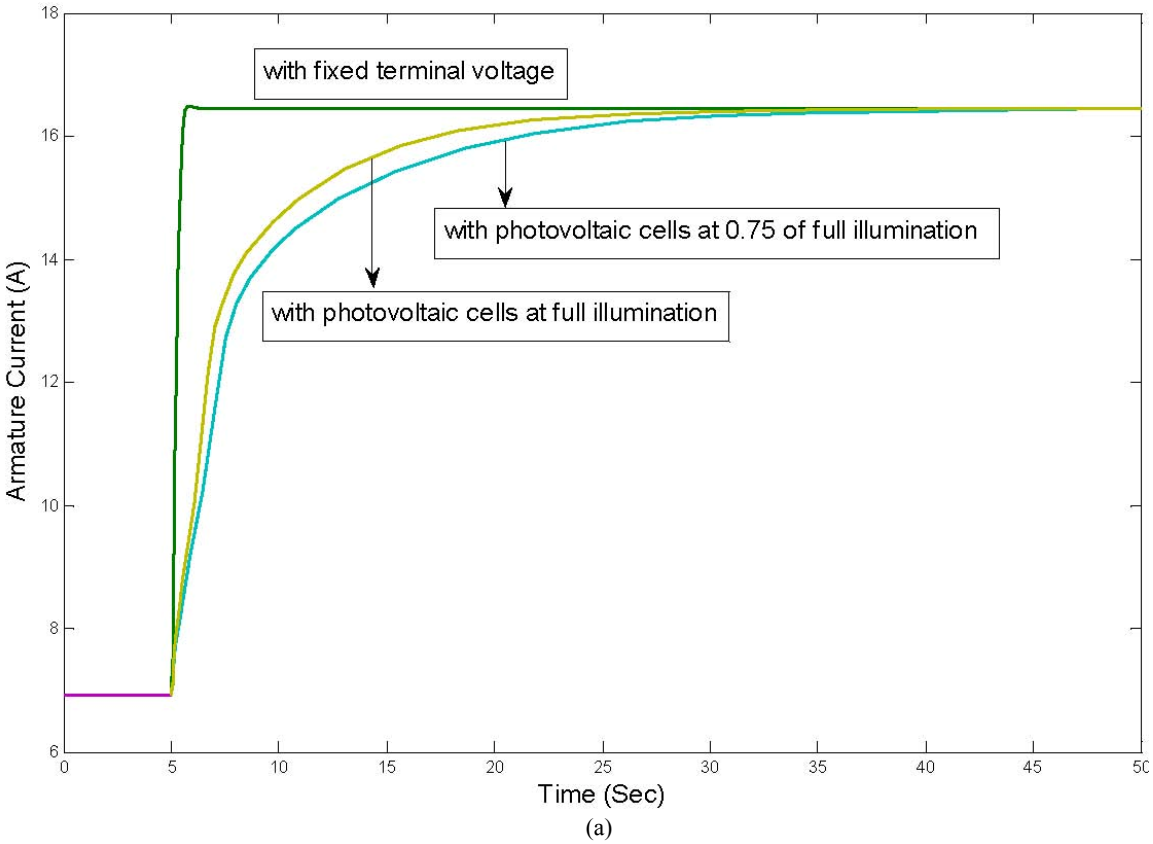

(a)

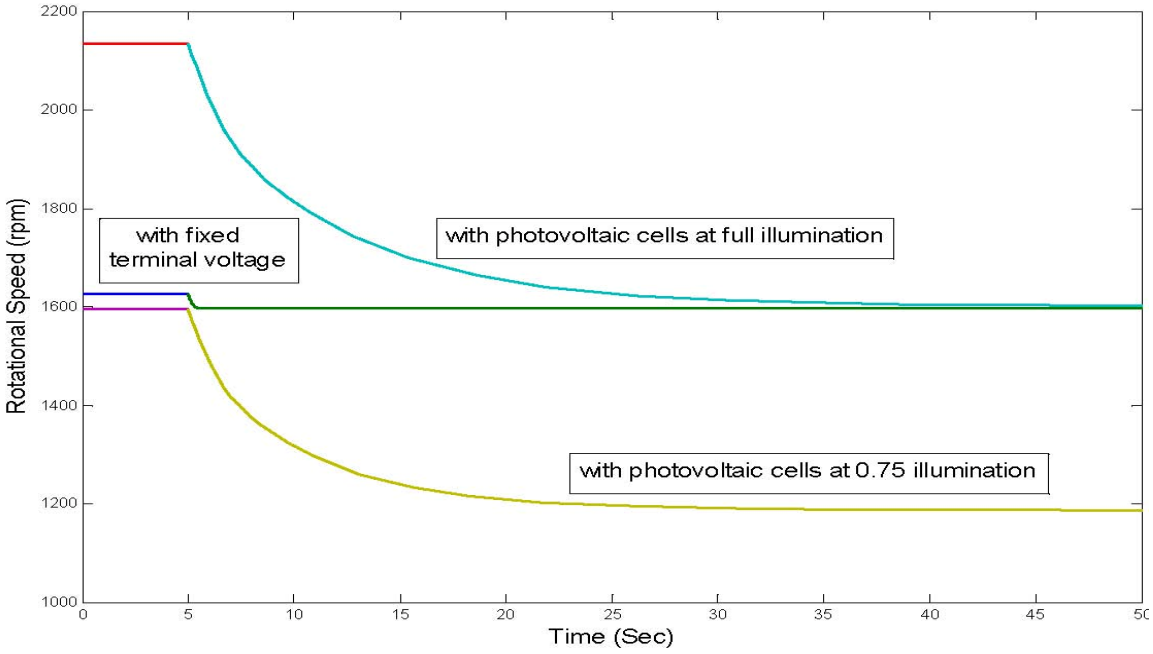

(b)

Figure 10: (a) Armature current and (b) rotational speed of the permanent-magnet DC motor after a step increase in the load torque from 5Nm to 11.9Nm.

4. Steady-State Output Characteristics

The steady-state output characteristics (torque-speed characteristics) of the three motors when fed by fixed terminal voltage and photovoltaic cells at different illuminations are studied. The operating points of the systems are obtained by dropping out all the time derivative terms of the dynamical differential equations and solving the resulting nonlinear algebraic equations. This has been carried out using the MATLAB Symbolic Math Toolbox instruction 'solve'. Figure 11 shows the torque-speed characteristics of the DC shunt motor and, Figure 12 shows that of the DC series motor and Figure 13 shows that of the permanent-magnet DC motor. Clearly, at the rated load torque the rotational speed of the motors in both cases are in good agreement as the terminal voltage of the photovoltaic cells at full illumination is very close to the rated voltage supplied in case of fixed terminal voltage. At lighter loads, the speed in case of photovoltaic cells is higher for the motors at full illumination. This takes place because the terminal voltage of the photovoltaic cells is higher at light loads as the current withdrawn from the cells is lower. In all cases, the characteristics in case of 0.75 of the full illumination is lower as the voltage supplied by PV cells is smaller.

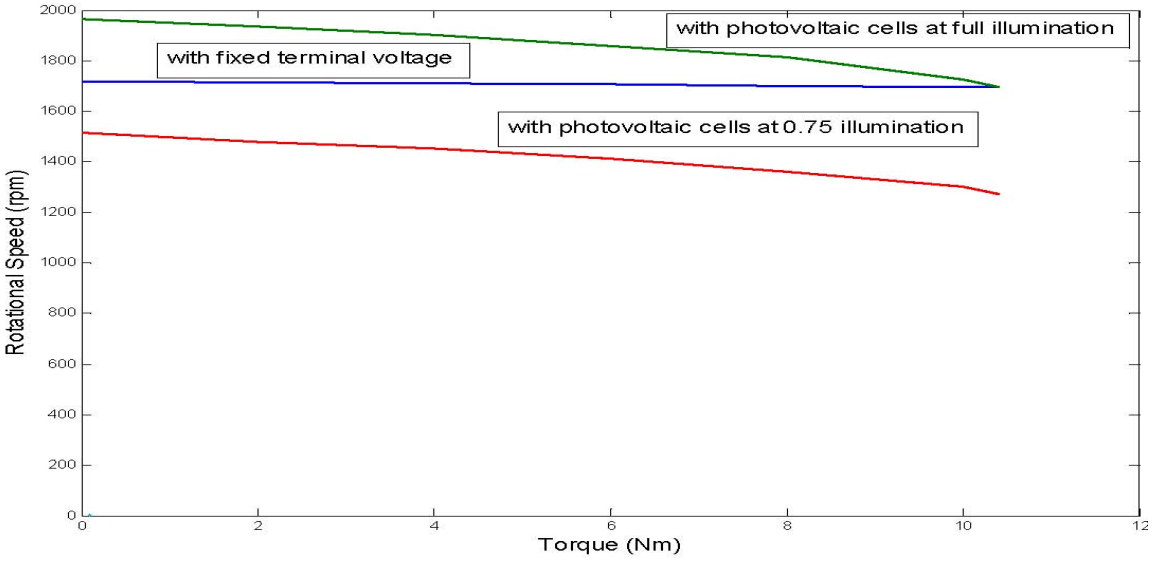

Figure 11. Torque-speed characteristics of DC shunt motor with photovoltaic cells at different illuminations and fixed terminal voltage

Figure 11. Torque-speed characteristics of DC shunt motor with photovoltaic cells at different illuminations and fixed terminal voltage

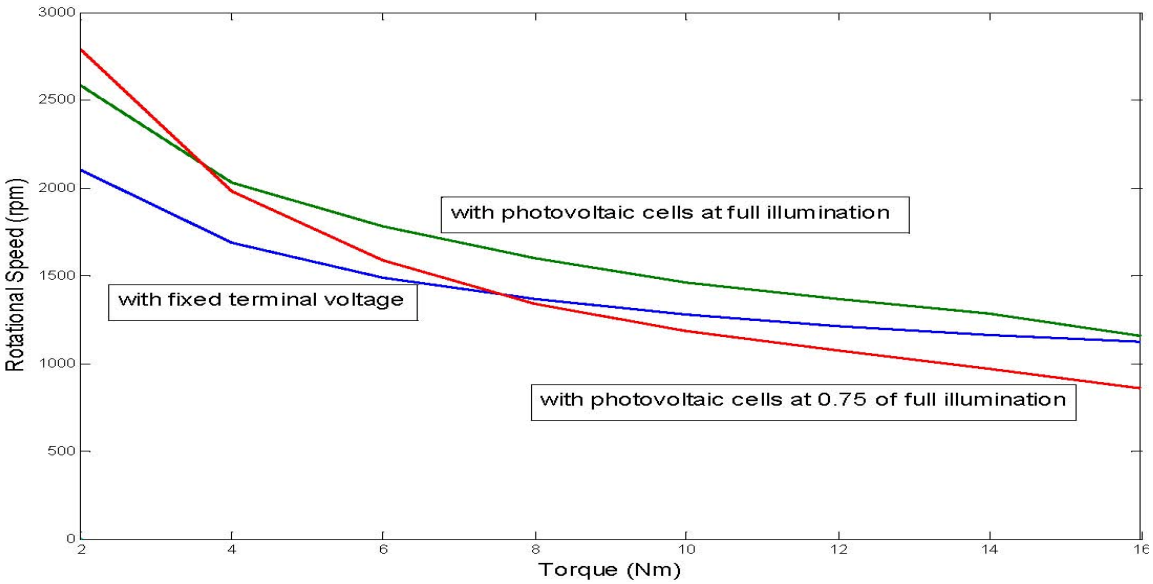

Figure 12. Torque-speed characteristics of DC series motor with photovoltaic cells at different illuminations and fixed terminal voltage

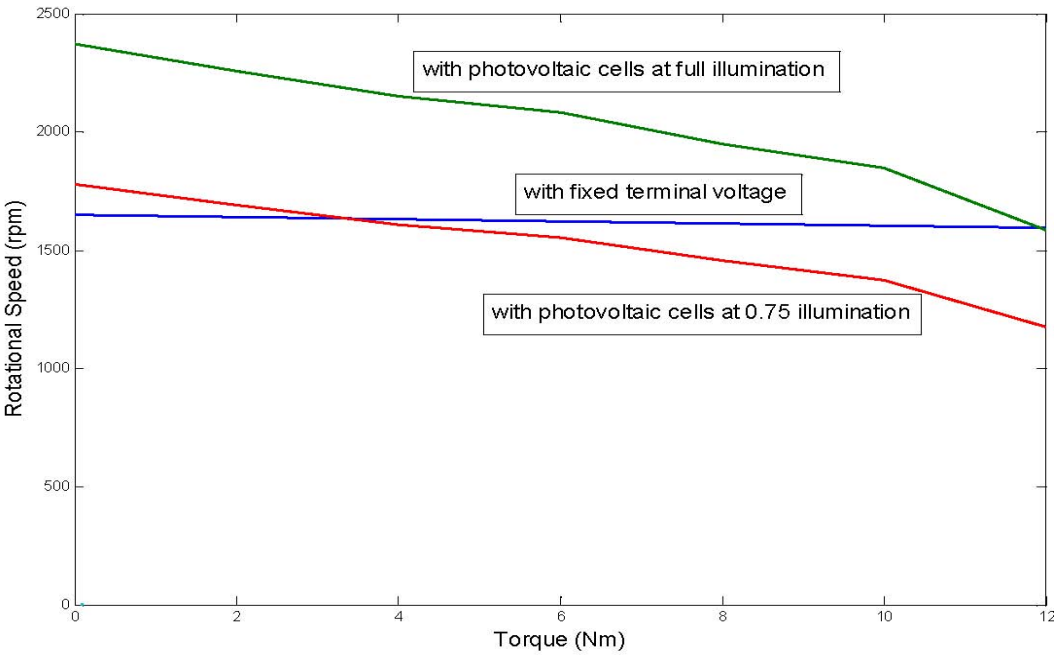

Figure 13.Torque-speed characteristics of permanent-magnet DC motor with photovoltaic cells at different illuminations and fixed terminal voltage .

5. Conclusions

The dynamical analysis of PV-powered DC shunt, series and permanent-magnet motors are studied. At the full solar intensity, the photovoltaic cells are designed to provide their maximum power at the rated conditions of the machine. The simulation results at two solar intensities are compared with the case of supplying the motors by fixed terminal voltage. The nonlinearity of the output characteristics of the photovoltaic cells and that of the magnetization curve of the DC machines are included in all simulations by polynomial curve fitting. The results show that when the machine is run at the rated conditions, the steady-state values are in good agreement in both cases of fully illuminated photovoltaic cells and fixed terminal voltage. At light loads with photovoltaic cells and full illumination, the responses of the machines are higher as the voltage supplied is higher. The output steady-state characteristics, torque-speed characteristics, of the three motors are outlined and compared in the cases of feeding them by fully illuminated solar cells, partially illuminated solar cells and fixed terminal voltage. All simulations are carried out using MATLAB.

References

[1] A. Al Tarabsheh, "Amorphous Silicon Based Solar Cells", Doctoral Diss., Institute of Physical Electronics, University of Stuttgart, Stuttgart, Germany, 2007.

[2] M. Bello and I. Davidson, "Dynamics of Solar-Powered Fractional Horse Power Motor", Int. Conf. on Electrical and Electronics Engineering, 7-9 , 2005, 273-277.

[3] M. Akbaba and M. C. Akbaba, "Dynamic Performance of a Photovoltaic-Boost Converter Powered DC Motor-Pump System", IEEE Int. Conf. Electrical Machines and Drives, 2001, 356-361.

[4] V. Badescu, "Dynamic Model of a Complex System Including PV cells, Electric Battery, Electrical Motor and Water Pump", Solar Energy, Vol. 28, 2003, 1165-1181.

[5] W. Anis and H. M. B. Metwally, "Dynamic Performance of a Directly Coupled PV Pumping System", Solar Energy, Vol. 53, No. 3, 1994.

[6] H. M. Metwally and W. R. Anis, "Dynamic Performance of Directly Coupled Photovoltaic Water Pumping System Using D.C. Shunt Motor", Energy Convers. Mgm. Vol. 37, No. 9, 1996, 1407-1416,.

[7] H. Hilmer, A. Ratka, K. Vajen, H. Ackermann, W. Fuhs and O. Melsheirner, "Investigation of Diretly Coupled Photovoltaic Pumping System Connected to a Large Absorber Filed", Solar Energy, Vol. 61, 1997, 65-76.

[8] M. Akbaba, I. Qamber and A. Kamal, "Matching of Separately Excited DC Motor to Photovoltaic Generators for Maximum Power Output", Solar Energy, Vol. 63, 1998, 375-385.

[9] M. Akbaba, "Matching Induction Motors to PVG for Maximum Power Transfer", The 9th Arab Int. Conf. Solar Energy , Vol. 209, 2007, 31-38.

[10] A. Betka and A. Moussi, "Performance Optimization of a Photovoltaic Induction Motor Pumping System" Renewable Energy, Vol. 29, 2004, 2167-2181.

[11] C. Hua, J. Lin and C. Shen, "Implementation of a DSP Controlled Photovoltaic System with Peak Power Tracking", IEEE Trans. Ind. Electronics, Vol. 45, No. 1, 1998, 99-107.

[12] E. Muljadi, "PV Water Pumping with a Peak Power Tracker Using a Simple Six Step Square-Wave Inverter", IEEE Trans. Industrial Applications, Vol. 33, No. 3, 1997, 714-721.

[13] C.L.P. Swamy, B. Singh and B.P. Singh, "Dynamic Performance of a Permanent Magnet Brushless DC Motor Powered by a PV Array for Water Pumping", Solar Energy Mater, Solar Cells, Vol. 36, 1995, 187-200.

[14] L. D. Partain, Solar cells and their applications, John Wiley & Sons, Inc., 1995.

[15] Chee-Mun Ong, Dynamic Simulation of Electric Machinery, Prentice Hall PTR, Upper Saddle River, New Jersy 07458, 1998.

[16] M. S. Widyan, "Design, Optimization, Construction and Test of Rare-Earth Permanent-Magnet Electrical Machines with New Topology for Wind Energy Applications", Doctoral Diss., Institute of Energy and Automation Technology, Berlin University of Technology, Germany, 2006.

[17] J. Merten, M. Asensi, C. Voz, A. V. Shah, R. Platz, and J. Andreu, "Equivalent Circuit and Analytical Analysis of Amorphous Silicon Solar Cells and Modules", IEEE Transactions on Electron Devices Vol. 45, 1998, 423.

[18] R. M. Swanson, Handbook of Photovoltaic Science and Engineering, edited by A. Luque and S. Hegedus, Wiley, West Sussex, England, 2003.

Appendix A

1) The numerical parameters of the DC shunt motor are:

$L_F = 10H$, $R_F + R_{adj} = 80 \rightarrow 120\Omega$, $V = 125V$, $L_a = 18mH$, $R_a = 0.24\Omega$, $J = 0.5kgm^2$.

2) The numerical parameters of the DC series motor are:

$L_F = 44mH$, $R_F = 0.2\Omega$, $V = 125V$, $L_a = 18mH$, $R_a = 0.24\Omega$, $J = 0.5kgm^2$.

3) The numerical parameters of the permanent-magnet DC motor are:

$L_a = 18mH$, $R_a = 0.24\Omega$, $K_m = 0.7237$ Vs, $V = 125V$, $J = 0.5kgm^2$.